PHYSICAL REVIEW B **91**, 100503(R) (2015)

Vortex arrays in nanoscopic superfluid helium droplets

Francesco Ancilotto,[1,2] Martí Pi,[3] and Manuel Barranco[3]
[1]*Dipartimento di Fisica e Astronomia "Galileo Galilei" and CNISM, Università di Padova, via Marzolo 8, 35122 Padova, Italy*
[2]*CNR-IOM Democritos, via Bonomea, 265-34136 Trieste, Italy*
[3]*Departament ECM, Facultat de Física, and IN^{2}UB, Universitat de Barcelona. Diagonal 645, 08028 Barcelona, Spain*
(Received 26 January 2015; revised manuscript received 3 March 2015; published 23 March 2015)

We have studied the appearance of vortex arrays in a rotating ^{4}He nanodroplet at zero temperature within density functional theory. Our results are compared with those for classical rotating fluid drops used to analyze the shape and vorticity in recent experiments [L. F. Gomez *et al.*, Science **345**, 906 (2014)], where vortices have been directly seen in superfluid droplets for the first time. In agreement with the experiments, we have found that the shape of the droplet changes from pseudospheroid, oblatelike for a small number of vortices to a peculiar "wheel-like" shape, delimited by nearly flat upper and lower surfaces, when the number of vortices is large. Also in agreement with the experiments, we have found that the droplet remains stable well above the stability limit predicted by classical theories for axially symmetric shapes.

DOI: 10.1103/PhysRevB.91.100503 PACS number(s): 67.25.dk, 67.25.dr

Helium-4 droplets created by expanding a cold helium gas [1] or fragmentation of a cryogenic liquid attain a limiting temperature below 0.4 K [2], and constitute the only self-bound superfluid systems. Superfluidity in helium droplets was established through the dissipationless rotation of a carbonyl sulfide (OCS) molecule inside them, as indicated by the appearance of a clean rovibrational spectrum [3]. More recently, indirect evidence of quantum vortices [4–6] and the existence of a critical Landau velocity below which impurities displace inside helium droplets without experiencing any friction [7] point towards a superfluid character of helium nanodroplets.

If a rotating helium droplet in the normal phase above the superfluid transition temperature $T_\lambda = 2.17$ K is cooled down, reaching the superfluid phase, it reacts by storing its angular momentum either into quantized vortices or into traveling capillary waves [8]. Conversely, a critical angular velocity ω_c has to be supplied to the superfluid droplet for the nucleation of vortices with quantized velocity circulation in units of h/M, where h is the Planck constant and M is the mass of a ^{4}He atom. Single vortices in helium droplets have been addressed theoretically by methods of different complexity (see, e.g., Refs. [9–13]).

When the angular velocity is increased above ω_c, larger amounts of angular momentum may be stored into the superfluid by increasing the number of nucleated vortices. These vortices arrange themselves into ordered structures (lattices) whose existence in bulk superfluid ^{4}He was established long ago [14,15]. We refer the reader to Refs. [16–18] for a general presentation of the subject.

Very recently, superfluid He nanoscopic droplets in fast rotation have been studied by coherent x-ray scattering [19]. The existence of vortex lattices inside the droplets was established by the appearance of Bragg patterns from Xe clusters trapped in the vortex cores in droplets made of $N = 10^8$–10^{11} atoms (corresponding to radii from 100 to 1000 nm) produced by the fragmentation of liquid helium expanding into vacuum. The shapes of the droplets were consistent with those of axially symmetric oblate pseudospheroids with a large aspect ratio (AR), defined as the ratio of the long half-axis length b to the short half-axis length a along the rotational axis. While normal liquid drops change their shape as rotation becomes faster [20–22] to resemble a "peanut" (multilobe shape) or a "blood cell," no evidence of such shape shifting has been seen in helium nanodroplets [19]. As shown in the following, this is fully confirmed by our calculations.

The presence of dopants was instrumental for detecting the vortex cores, although their number was sensibly smaller than the number of helium atoms ($N_{\rm Xe} \sim 10^{-3} N_{\rm He}$) and their presence is not expected to introduce large deformations in the droplet despite the fact that they locally distort the superfluid around them (see, e.g., Refs. [10,23]). Possible effects on the distribution of vortex cores inside the droplet might come from the additional rotational energy associated to the Xe mass, especially at the periphery of the droplet. Although such effects seem to have been observed occasionally in the experimental images of Ref. [19], we will not consider them here. In the case of a rotating nanocylinder, these distortions were found to be negligible [23].

Once the presence of a vortex lattice in a droplet of aspect ratio b/a is experimentally established, the number N_v of vortices in the lattice could be determined approximately from the vortex areal density (Feynman's formula [24])

$$n_v \equiv N_v/\mathcal{S} = 2M\omega/h, \tag{1}$$

where ω is the rotational angular velocity and $\mathcal{S} = \pi b^2$ is the equatorial cross section of the droplet. Since ω cannot be directly determined in the experiment [19], the analysis relies on the classical relationship between the AR —experimentally accessible through the diffraction contour maps—and the angular velocity, whose connection with the parameters a and b is given by the classical theories of rotating liquid drops [20,21]. In this way the experiments estimated that the number of vortices in a single droplet could be as large as $N_v = 160$. When the vortex density is particularly large, the experimental images showed also the occurrence of "wheel-shaped" droplets [19], which have no classical counterpart.

The distinct features of superfluid helium, namely, its irrotational flow and the possible appearance of quantized vortices, are of course not included in the classical rotating droplet model [20,21]. The existence of a large vortex lattice

might influence the appearance of the rotating droplet, and the irrotational moment of inertia is known to be very different from that of the rigid body [25]. These facts call for theoretically addressing rotating helium droplets with accurate methods which have proven to provide reliable results for superfluid ^{4}He in confined geometries.

We present here a density functional theory (DFT) study at zero temperature of pure superfluid helium droplets hosting an increasing number of vortices. A previous attempt to study multivortex configurations in superfluid droplets is described in Ref. [26], where a simplified model assuming linear vortices and a rigid spherical droplet was used.

We have recently analyzed a simpler model system, namely, a rotating superfluid ^{4}He nanocylinder hosting arrays of linear vortex lines [23], that constitutes the starting point of the present study. Within our approach, a self-bound superfluid ^{4}He droplet is described by a complex effective wave function $\Psi(\mathbf{r},t)$ related to its atomic density as $\rho(\mathbf{r},t) = |\Psi(\mathbf{r},t)|^2$. In the fixed-droplet frame of reference (corotating frame) we seek for stationary solutions $\Psi(\mathbf{r},t) = e^{-\imath\mu t/\hbar}\Phi(\mathbf{r})$, where the chemical potential μ and the time-independent effective helium wave function Φ are obtained by solving the time-independent equation

$$[\hat{H} - \omega\hat{L}_z]\Phi(\mathbf{r}) = \mu\Phi(\mathbf{r}), \tag{2}$$

where $\hat{H}$ is the DFT Hamiltonian [27], $\hat{L}_z$ is the angular momentum operator around the z axis, and ω is the angular velocity of the corotating frame.

To determine $\Phi(\mathbf{r})$ describing a configuration where N_v vortex lines are present, we follow the "imprinting" strategy, i.e., we start the imaginary-time evolution of Eq. (2) leading to the minimum energy configuration with a helium wave function [23]

$$\Phi_0(\mathbf{r}) = \sqrt{\rho_0(\mathbf{r})}\sum_{j=1}^{N_v}\left[\frac{(x-x_j)+i(y-y_j)}{\sqrt{(x-x_j)^2+(y-y_j)^2}}\right], \tag{3}$$

where $\rho_0(\mathbf{r})$ is the density of the vortex-free droplet and (x_j, y_j) is the initial position of the j-vortex linear core with respect to the z axis of the droplet. During the functional minimization the vortex positions will change to provide, at convergence, the lowest energy vortex configuration. It is worth stressing that we work in Cartesian coordinates and that no symmetry is imposed to the solutions of Eq. (2), and thus during the imaginary-time evolution both the initial vortex positions and their geometry change (the initial linear vortices become eventually more or less bent—see Fig. 1). We checked that different initial positions of the vortices in the "imprinted" wave function produce, for a given rotational frequency, the same final configuration, thus excluding any bias in the results. We refer the reader to Ref. [23] and references therein for technical details on how this equation has been solved.

While it is known [9] that vortex nucleation is hindered by free energy barriers, the imprinting technique does not allow one to say anything about their heights: A proper study of the energy barrier for nucleation implies a full real-time study of droplet rotation, which is beyond the scope of our Rapid Communication.

Due to the high computational cost of our calculations, we have limited this study to a helium droplet made of $N_{\mathrm{He}} =$ 15 000 helium atoms having a radius $R = r_0 N_{\mathrm{He}}^{-1/3}$ with $r_0 =$ 2.22 Å, i.e., $R = 54.7$ Å. This droplet is still much smaller than the experimental ones, which in turn limits the number of hosted vortices. However, our findings can be compared with the experimental results on much larger droplets once scaled with a dimensionless characteristic rotational velocity Ω defined as [21]

$$\Omega = \sqrt{\frac{M\rho_0 R^3}{8\gamma}}\omega, \tag{4}$$

where $\rho_0 = 0.0218\,\text{Å}^{-3}$ is the helium atom density and $\gamma =$ $0.274\,\text{K Å}^{-2}$ is the surface tension of the liquid. For the $N_{\mathrm{He}} =$ 15 000 droplet, $\Omega = 1$ corresponds to $\omega = 1.13 \times 10^{10}\ \text{s}^{-1}$.

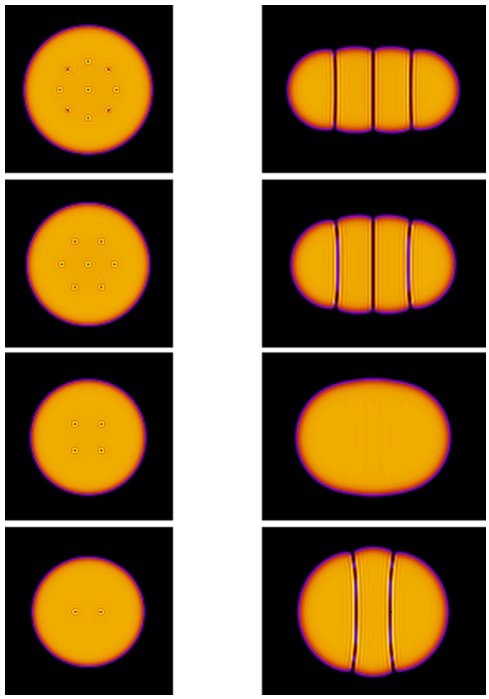

FIG. 1. (Color online) Helium droplet configurations hosting (from bottom to top) $N_v = 2$, 4, 7, and 9 vortices. The left column shows the density in the $z = 0$ symmetry plane (top view), while the right column shows side views ($x = 0$ plane).

Figure 1 shows configurations hosting $N_v = 2$, 4, 7, and 9 vortex arrays obtained with $\Omega = 0.43$, 0.54, 0.62, and 0.69, respectively. Comparing the top and lateral views, it is apparent that the droplet becomes increasingly deformed, oblatelike, as N_v (and thus Ω) increases. Also apparent is how the droplet surface locally deforms and the vortex lines bend, forced by the physical requirement that their open ends hit the surface perpendicularly. The bending is smaller for larger N_v and, at variance with the classical droplet results [20–22], the droplet becomes "wheel-like," as indeed observed in the experiments [19].

By increasing the angular velocity, the number of vortices that can be stabilized inside the droplet increases. Eventually, a maximum number of vortices can be hosted, above which the rotating droplet will no longer be stable. For the $N_{\mathrm{He}} = 15\,000$ droplet we have found that the maximum N_v value is 9.

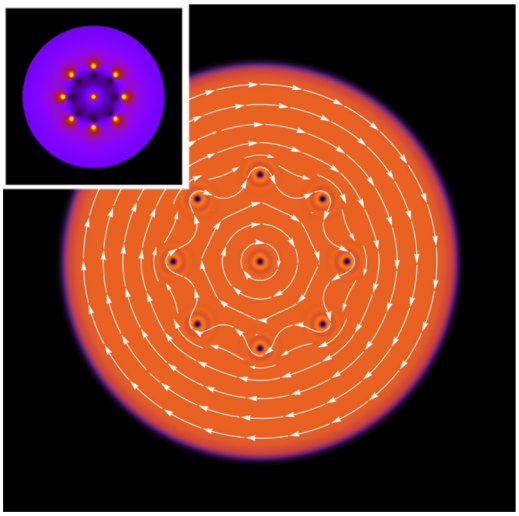

FIG. 2. (Color online) Circulation lines of the velocity field corresponding to the $N_v = 9$ configuration of Fig. 1. The inset displays in a color scale the regions around the vortex cores where the modulus of the velocity field is higher (bright spots). The dark spots are regions of low vorticity due to the interference between the velocity fields of neighboring vortices.

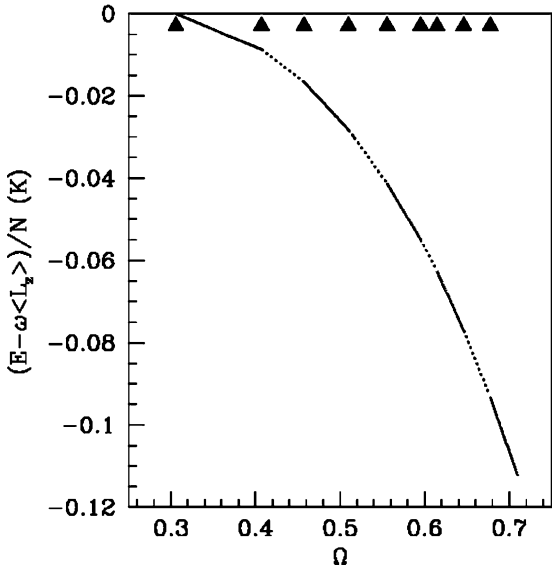

FIG. 3. Stability diagram for a number of vortex lines $N_v = 0,1,2,\ldots,9$ as a function of the dimensionless angular velocity Ω. The zero of the energy scale corresponds to the energy of the vortex-free droplet. The vertical axis is the energy per atom in the corotating frame referred to that of the vortex-free droplet. The triangles mark the crossings between different stability lines.

The higher the angular velocity, the more packed the vortex array is around the rotation axis. This leaves a "strip" around the equator of the droplet that is free of vortices that can be clearly appreciated in the $N_v = 9$ case, as shown in Fig. 2, where we display several circulation lines of the superfluid velocity field. The inset shows in a color scale the regions around the vortex cores where the modulus of the velocity field is higher (bright spots). As expected, the calculated circulation of the velocity field of the superfluid along a path surrounding the vortex array equals N_v, and equals unity around every single vortex.

Figure 3 shows the calculated stability diagram. As for the rotating bucket [23,28,29], the energetically favored structures for $N_v > 5$ are made of a ring of vortices encircling a vortex at the center of the droplet.

It is worth observing that Eq. (1), which strictly applies to an extended vortex triangular (Abrikosov) lattice made of a large number of vortex lines, is also fulfilled in the present case in spite of the limited number of vortices. This occurs in the case of $N_v = 7$, where the equilibrium structure (see Fig. 1) is a "patch" of a triangular lattice whose areal density is $n_v = 2/(\sqrt{3}d^2)$, d being the mean intervortex distance. By equating this expression to Eq. (1)—with the value $\Omega = 0.62$ used to obtain the seven-vortex configuration shown in Fig. 1—one gets $d = 28.3$ Å. An average vortex-vortex distance $d = 28.2$ Å can be estimated from Fig. 1, which compares very well with the result of the classical vortex theory [20–22].

Figure 1 shows that, disregarding the vortex array, the shape of the droplet is almost axially symmetric. To determine its AR we have calculated a and b from the moments of the density distribution, obtaining [30] $b/a = [\langle x^2\rangle/\langle z^2\rangle]^{1/2}$, where $\langle x^2\rangle = \int \rho(\mathbf{r})x^2 d\mathbf{r}$ and $\langle z^2\rangle = \int \rho(\mathbf{r})z^2 d\mathbf{r}$.

The AR dependence on the angular velocity Ω is shown in Fig. 4, together with the curve derived from the classical model for a rotating liquid droplet [20], and used in Ref. [19] to fit their data. Although the angular velocity in free nanoscopic droplets is difficult to control (and thus a more convenient independent variable would be the angular momentum), we use Ω as the independent variable in Fig. 4 for the sake of comparison with the results of Ref. [19] (solid line). Moreover, fixing the angular momentum of the droplet is computationally more involved, as it requires one to iterate on the angular velocity to get the desired L value.

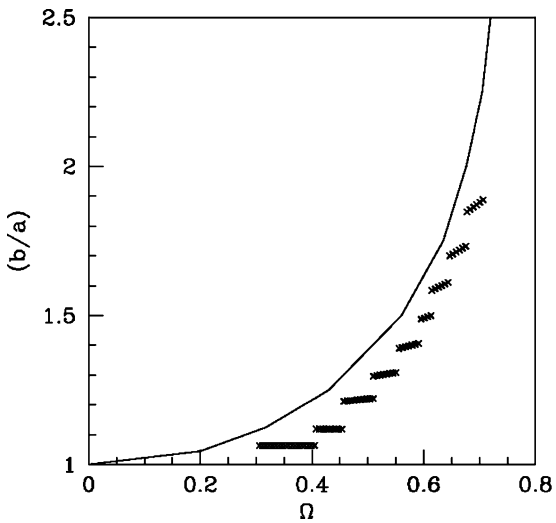

FIG. 4. Calculated aspect ratio b/a as a function of the dimensionless angular velocity Ω. The solid line shows the fit to the experimental (b/a) data reported in Ref. [19], obtained from the classical model for axisymmetric rotating droplets [20].

The figure shows that for a given angular velocity, the classical droplet model overestimates the calculated aspect ratio. Most likely, the calculated points in Fig. 4 should get closer to the classical curve for larger droplets having many vortices, which unfortunately are beyond the current possibilities of the DFT approach. Notice also that in the experiments of Ref. [19] axially symmetric stable droplets were observed with aspect ratios as high as $b/a = 2.3$, corresponding to $\Omega = 0.71$, considerably larger than the shape instability threshold of classical droplets leading to multilobe configurations, $\Omega = 0.56$. Our calculations also yield a similar behavior.

It appears from Fig. 4 that as N_v increases, the dependence of the AR on Ω within the corresponding stability region (i.e., within each group of crosses shown in Fig. 4) becomes increasingly important, i.e., the droplet is more easily deformed. Such an increase of the AR proceeds by the flattening of the droplet as the vortex cores are pushed, as the frequency is increased, towards the center of the droplet.

Another interesting difference between classical and superfluid behavior, which is likely related to the deviations from classical theory just discussed, emerges if we look at the ratio between the moment of inertia around the z axis, I_z calculated from the droplet mass distribution, and that obtained from the response of the superfluid to rotation, $I_\omega = \langle \hat{L}_z \rangle / \omega$. The ratio I_ω/I_z is shown in Fig. 5 as a function of N_v, taking for Ω a value in the middle of each stability region. One may notice that the higher the angular velocity, the closer the moment of inertia becomes to the rigid-body moment of inertia.

To summarize, within DFT we have shown that the shape of rotating helium droplets hosting a number of vortices evolves from spheroidal at low angular velocities to wheel-like at high angular velocities. On the one hand, multilobe configurations present in classical viscid droplets [22] are hindered by the appearance of vortex arrays whose regular distribution is hard to accommodate into peanutlike (or higher lobe number) shapes. On the other hand, the physical requirement that the ends of the vortex lines hit the droplet surface perpendicularly favors their parallel alignment for large vortex arrays, and hence the appearance of wheel-like shapes, as indeed observed in the experiments. Finally, in spite of the apparent differences between normal and superfluid rotating droplets, the classical relationship between the aspect ratio and the angular frequency is fairly fulfilled, the classical relationship underestimating the actual angular frequency by less than 10% for the relevant, larger vortex arrays. Thus, it can be used with some confidence in the analysis of the experimental results.

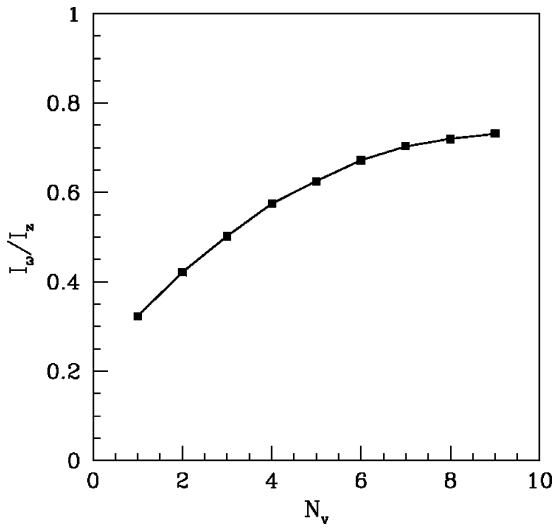

FIG. 5. Calculated ratio I_ω/I_z shown as a function of the number of vortices N_v.

We thank Andrey Vilesov for stimulating discussions. This work has been performed under Grants No. FIS2011-28617-C02-01 from DGI, Spain (FEDER) and No. 2014SGR401 from Generalitat de Catalunya.

[1] J. P. Toennies and A. F. Vilesov, Angew. Chem. Int. Ed. **43**, 2622 (2004).
[2] M. Hartmann, R. E. Miller, J. P. Toennies, and A. F. Vilesov, Phys. Rev. Lett. **75**, 1566 (1995).
[3] S. Grebenev, J. P. Toennies, and A. F. Vilesov, Science **279**, 2083 (1998).
[4] L. F. Gomez, E. Loginov, and A. F. Vilesov, Phys. Rev. Lett. **108**, 155302 (2012).
[5] E. Latimer, D. Spence, C. Feng, A. Boatwright, A. M. Ellis, and S. Yang, Nano Lett. **14**, 2902 (2014).
[6] Ph. Thaler, A. Volk, F. Lackner, J. Steurer, D. Knez, W. Grogger, F. Hofer, and W. E. Ernst, Phys. Rev. B **90**, 155442 (2014).
[7] N. B. Brauer, S. Smolarek, E. Loginov, D. Mateo, A. Hernando, M. Pi, M. Barranco, W. J. Buma, and M. Drabbels, Phys. Rev. Lett. **111**, 153002 (2013).
[8] A. Leal, D. Mateo, A. Hernando, M. Pi, and M. Barranco, Phys. Chem. Chem. Phys. **16**, 23206 (2014).
[9] G. H. Bauer, R. J. Donnelly, and W. F. Vinen, J. Low Temp. Phys. **98**, 47 (1995).
[10] F. Dalfovo, R. Mayol, M. Pi, and M. Barranco, Phys. Rev. Lett. **85**, 1028 (2000).
[11] K. K. Lehmann and R. Schmied, Phys. Rev. B **68**, 224520 (2003).
[12] F. Ancilotto, M. Barranco, and M. Pi, Phys. Rev. Lett. **91**, 105302 (2003).
[13] E. Sola, J. Casulleras, and J. Boronat, Phys. Rev. B **76**, 052507 (2007).
[14] W. F. Vinen, Proc. R. Soc. London, Ser. A **260**, 218 (1961).
[15] G. A. Williams and R. E. Packard, Phys. Rev. Lett. **33**, 280 (1974).
[16] R. J. Donnelly, *Quantized Vortices in Helium II*, Cambridge Studies in Low Temperature Physics (Cambridge University Press, Cambridge, U.K. 1991), Vol. 3.
[17] L. Pitaevskii and S. Stringari, *Bose-Einstein Condensation*, International Series of Monographs on Physics Vol. 116 (Clarendon, Oxford, U.K., 2003).
[18] A. L. Fetter, Rev. Mod. Phys. **81**, 647 (2009).
[19] L. F. Gomez *et al.*, Science **345**, 906 (2014).
[20] S. Chandrasekhar, Proc. R. Soc. London, Ser. A **286**, 1 (1965).

[21] R. A. Brown and L. E. Scriven, Proc. R. Soc. London, Ser. A **371**, 331 (1980).
[22] R. J. A. Hill and L. Eaves, Phys. Rev. Lett. **101**, 234501 (2008).
[23] F. Ancilotto, M. Pi, and M. Barranco, Phys. Rev. B **90**, 174512 (2014).
[24] R. P. Feynman, in *Progress in Low Temperature Physics*, edited by C. J. Gorter (North-Holland, Amsterdam, 1955), Vol. 1, p. 1.
[25] A. Bohr and B. R. Mottelson, *Nuclear Structure* (Benjamin, Reading, MA, 1975), Vol. II, Appendix 6A.
[26] S.-T. Nam, G. H. Bauer, and R. J. Donnelly, J. Korean Phys. Soc. **29**, 755 (1996).
[27] F. Ancilotto, M. Barranco, F. Caupin, R. Mayol, and M. Pi, Phys. Rev. B **72**, 214522 (2005).
[28] G. B. Hess, Phys. Rev. **161**, 189 (1967).
[29] L. J. Campbell and R. M. Ziff, Phys. Rev. B **20**, 1886 (1979).
[30] We have verified that this gives the same AR as computed by direct inspection of the equidensity contour-line plots obtained from our calculations.